Original Article

MOLECULAR METABOLISM

Nipsnap1—A regulatory factor required for long-term maintenance of non-shivering thermogenesis

Yang Liu [1,4], Yue Qu [1,4], Chloe Cheng [2], Pei-Yin Tsai [1], Kaydine Edwards [1], Siwen Xue [1], Supriya Pandit [1], Sakura Eguchi [1], Navneet Sanghera [3], Joeva J. Barrow [1,*]

ABSTRACT

Objective: The activation of non-shivering thermogenesis (NST) has strong potential to combat obesity and metabolic disease. The activation of NST however is extremely temporal and the mechanisms surrounding how the benefits of NST are sustained once fully activated, remain unexplored. The objective of this study is to investigate the role of 4-Nitrophenylphosphatase Domain and Non-Neuronal SNAP25-Like 1 (Nipsnap1) in NST maintenance, which is a critical regulator identified in this study.

Methods: The expression of Nipsnap1 was profiled by immunoblotting and RT-qPCR. We generated Nipsnap1 knockout mice (N1—KO) and investigated the function of Nipsnap1 in NST maintenance and whole-body metabolism using whole body respirometry analyses. We evaluate the metabolic regulatory role of Nipsnap1 using cellular and mitochondrial respiration assay.

Results: Here, we show Nipsnap1 as a critical regulator of long-term thermogenic maintenance in brown adipose tissue (BAT). Nipsnap1 localizes to the mitochondrial matrix and increases its transcript and protein levels in response to both chronic cold and β3 adrenergic signaling. We demonstrated that these mice are unable to sustain activated energy expenditure and have significantly lower body temperature in the face of an extended cold challenge. Furthermore, when mice are exposed to the pharmacological β3 agonist CL 316, 243, the N1—KO mice exhibit significant hyperphagia and altered energy balance. Mechanistically, we demonstrate that Nipsnap1 integrates with lipid metabolism and BAT-specific ablation of Nipsnap1 leads to severe defects in beta-oxidation capacity when exposed to a cold environmental challenge.

Conclusion: Our findings identify Nipsnap1 as a potent regulator of long-term NST maintenance in BAT.

Keywords Nipsnap1; Thermogenesis maintenance; Brown adipose tissue; Lipid metabolism; Energy expenditure

1. INTRODUCTION

The metabolic state of obesity results from the chronic and excessive accumulation of fat either due to overnutrition and/or insufficient energy expenditure [1,2]. It is well-established that obesity is associated with adverse health outcomes including diabetes, cardiovascular diseases, and several types of cancer [3—6]. Indeed, the global prevalence of obesity in humans has reached pandemic proportions and it is now classified as the leading cause of preventable death worldwide [7]. Current therapies such as dietary restriction, surgery, or pharmacological interventions are either unsustainable or are limited by adverse side effects [8—11]. Therefore, the need for novel therapeutic options is critical. The activation of the brown and beige fat non-shivering thermogenesis (NST) program to increase energy expenditure has been conclusively proven to protect against obesity in rodent models and is promising as a molecular treatment option to combat obesity in humans [12—15]. Indeed, human brown adipose tissue (BAT) can be safely activated by acute cold exposure and is associated with an increase in energy expenditure [16—21]. While the mechanisms underlying BAT thermogenic activation are increasingly well understood, the mechanisms regarding how NST is sustained once activated are poorly characterized and relatively under-explored [22—24]. This knowledge gap becomes extremely important given the transient nature of BAT activation. As has been shown in human studies, once thermogenic stimuli are removed, BAT is rapidly deactivated and most protective benefits against obesity are lost [25,26]. Identifying regulatory factors that are required for long-term thermogenic maintenance will provide additional molecular therapeutic opportunities to maintain the protective benefits of NST in order to combat obesity and associated metabolic diseases. In order to address this problem, we have mapped the BAT mitochondrial proteome in mice under chronic cold challenge conditions to identify unique proteins that either become upregulated or demonstrate sustained upregulation in late-stage thermogenesis—defined as greater than or

[1]Division of Nutritional Sciences, Cornell University, Ithaca, NY, 14850, USA [2]Department of Veterinary Medicine, Cornell University, Ithaca, NY, 14850, USA [3]Department of Biological Sciences, San Jose State University, San Jose, CA, 95192, USA

[4] Co-First Author.

*Corresponding author. E-mail: jb2254@cornell.edu (J.J. Barrow).

Received February 16, 2023 • Revision received June 29, 2023 • Accepted June 30, 2023 • Available online 7 July 2023

https://doi.org/10.1016/j.molmet.2023.101770

List of Abbreviations

Nipsnap1	4-Nitrophenylphosphatase Domain and Non-Neuronal SNAP25-Like 1
N1—KO	Nipsnap1 Knockout Mice
N1-Flox	Nipsnap1 Flox Mice
NST	Non-Shivering Thermogenesis
TN	Thermoneutrality
VO2	Volume of inspired oxygen
VCO2	Volume of expelled carbon dioxide
RER	Respiratory Exchange Ratio
BAT	Brown Adipose Tissue
IWAT	Inguinal White Adipose Tissue
gWAT	Gonodal White Adipose Tissue
GTT	Glucose Tolerance Test
ITT	Insulin Tolerance Test

equal to 7 days of cold exposure. We hypothesize that proteins exhibiting this expression pattern could be involved in the regulation of long-term thermogenic maintenance in BAT.

Here, we have discovered a thermogenic factor known as 4-Nitrophenylphosphatase Domain and Non-Neuronal SNAP25-Like 1 (Nipsnap1) as a potent regulator of long-term thermogenic maintenance in BAT. Nipsnap1 is an evolutionarily conserved protein from flies to humans that is expressed predominantly in highly energetic tissues such as the brain and liver [27—31]. It possesses an N-terminal mitochondrial targeting sequence (MTS) that directs it to the mitochondrial matrix, and previous studies have determined that Nipsnap1 plays a critical role in mitophagy where it functions as a sensor of mitochondrial health and recruits autophagy proteins when mitochondria become damaged [32,33]. Other reported functions include its role in pyruvate and branched chain amino acid metabolism [34,35], pain transmission signaling, neurological disorders, carcinogenesis, and the immune response [36,37]. Most of the current research for Nipsnap1 however details these functions in brain or liver tissues but the expression profile and function of Nipsnap1 in thermogenic adipose tissue is unknown.

In this study, we provide evidence of Nipsnap1 as a late-stage thermogenic regulatory factor. We show that Nipsnap1 is robustly activated after chronic cold exposure or pharmacological β3 activation in BAT. We further demonstrate that loss-of-Nipsnap1 in brown fat depots impairs the sustained activation of the NST program. Mechanistically, ablation of Nipsnap1 in BAT compromises both cellular *de novo* lipogenesis and mitochondrial lipid beta-oxidation capacity leading to a significant decline in energy expenditure and a reduced ability to maintain body temperature homeostasis in the face of chronic cold exposure. Nipsnap1 may have targeted therapeutic opportunities to ensure the long-term activation of NST.

2. MATERIALS AND METHODS

2.1. Mice

All animal experiments were approved by the Institutional Animal Care and Use Committee (IACUC) at Cornell University. For all animal studies, both male and female mice were used as no specific gender differences were observed. The specific number and gender of the mice are indicated in each figure. To generate the conditional Nipsnap1 transgenic mice, genetic recombineering was performed as described previously [38]. Briefly, murine heterozygous Nipsnap1 sperm (EMMA Strain ID: EM 04250) harboring loxP sites between exons 2—4 of the Nipsnap1 gene was acquired from the European Conditional Mouse Mutagenesis Program (EUCOMM). *In vitro* fertilization (IVF) with Nipsnap1$^{Flox/wt}$ sperm and WT C57BL/6J mouse eggs was performed at the Cornell Stem Cell and Transgenic Core Facility. Live heterozygous Nipsnap1$^{Flox/wt}$ mice were subsequently crossed with mice harboring the FLP recombinase to remove the Neomycin cassette and inter-crossed to generate the homozygous floxed Nipsnap1$^{Flox/Flox}$ strain. To achieve thermogenic adipose tissue-specific deletion of Nipsnap1, Nipsnap1$^{Flox/Flox}$ mice were then crossed with UCP1 Cre mice (Jackson #024670). All mice were maintained on 12 h light and dark cycles and fed *ad libitum* with either standard irradiated rodent chow or a 60% high fat diet (HFD) (Research Diets D12492). For cold exposure experiments, 6-week-old male and female wild-type C57BL/6J (Jackson #000664) and Nipsnap1 transgenic mice were single-housed in rodent incubators and exposed to a constant temperature of 6.5 °C for indicated time points. For pharmacological induced thermogenesis experiments, mice were reared at room temperature (25 °C) until 6—8 weeks of age before being placed in the Promethion metabolic cages at TN where they were injected daily via intraperitoneal injection (IP) with 1 mg/kg CL 316,243 for the indicated time points. HFD treatment was initiated in mice at 6 weeks of age for 24 weeks.

2.2. Mouse primary brown adipocytes culture and differentiation

For *in vitro* studies of thermogenesis with primary brown adipocytes, BAT adipose tissue was obtained from 3-week-old male wild-type C57BL/6J mice or Nipsnap1 Flox mice. Fat pads from 5 mice were pooled after dissection, minced thoroughly and digested in 15 ml of BAT dissociation buffer (123 mM NaCl, 5 mM KCl, 1.3 mM $CaCl_2$, 5.0 mM Glucose, 100 mM HEPES, 4% BSA and 1.5 mg/ml collagenase B) for 30min at 37 °C with constant shaking. The cell suspension was filtered with a 100 μm cell strainer and centrifuged at 600 g for 5min. The pellet was then suspended in adipocyte culture medium (DMEM/F12 with 10% FBS, 25 mM HEPES, 1% PenStrep), filtered with a 40 μM cell strainer, centrifuged at 600 g for 5min, and resuspended in culture medium and plated in 10 cm polystyrene cell culture dishes. Preadipocytes were seeded to post confluency and differentiated with DMEM/F12 supplemented with 5ug/mL Insulin, 1 μM Rosiglitazone, 1 μM Dexamethasone, 0.5 mM Isobutylmethylxanthine and 1 nM T3. Cells were maintained in differentiation media for 48 h before being switched into maintenance media (5ug/mL Insulin and 1 μM Rosiglitazone and 1 nM T3) for 4—6 days. For primary brown adipocyte adenoviral-GFP or Cre treatment, primary Nipsnap1 flox brown adipocytes were treated with 1000 Multiplicity of infection (MOI) of either Adeno GFP or Adeno Cre virus for 72 h. Cells were then trypsinized and reseeded into desired assay plates and exposed to another dose of adenovirus treatment at an MOI of 1000 for 72 h. Cells were then differentiated as described above. For lipid signaling experiments, differentiated primary adipocytes were exposed to 1 μm of norepinephrine for 1 h before harvest.

2.3. Glucose and insulin tolerance tests

Glucose tolerance tests were performed at weeks 10 and 16 of the HFD treatment. Mice were fasted for 16 h before receiving 1.5 mg/kg intraperitoneal injection (IP) of glucose. Blood glucose levels were measured using a glucometer every 15min for a duration of 2 h after glucose administration. Insulin tolerance tests were performed at week 19 of the HFD treatment. Mice were fasted for 6 h prior to receiving 1U/kg IP injection of insulin. Blood glucose levels were then measured by

glucometer every 15min for a period of 2 h post-injection. The blood sample was collected from tail nicking.

2.4. *In vivo* indirect calorimetry

Mice were single-housed in rodent Promethion metabolic cages (Sable Systems International) situated in a temperature-controlled thermal cabinet with a 12-hour light/dark cycle schedule. For cold exposure studies, mice were reared at room temperature until 6 weeks of age. They were then acclimated in metabolic cages set to 30 °C for 72 h after which the thermal cabinet was cooled to 6 °C for the duration of the cold exposure study. For CL 316, 243 metabolic studies, mice were reared at room temperature until 8 weeks of age. They were then placed in the metabolic cages set to 30 °C for the duration of the experiment. CL 316,243 (Cayman #17499) was dissolved in PBS and injected into mice at 1 mg/kg bw daily for 10 days. Comprehensive real-time metabolic measurements such as energy expenditure (kcal/hr), oxygen consumption (VO_2), carbon dioxide expiration (VCO_2), locomotive movement (measured by X—Y infrared beam breaks), and respiratory exchange ratio (RER) were measured and recorded every 3 min using the Sable System data acquisition software (IM-3 v.20.0.3). Raw data was then processed using the Sable System Macro Interpreter software and One-Click Macro systems (v2.37). Data was further processed using the CalR software [39].

2.5. RNA and protein analyses

Total RNA was extracted using TRIzol reagent. Isolated tissues were homogenized using the Qiagen TissueLyser II in TRIzol to isolate total RNA and processed according to the manufacturer's instruction. Total RNA (1ug) was reverse transcribed to cDNA using the qScript cDNA Synthesis kit. RT-qPCR was performed using the CFX384 Real-Time PCR System using SYBR Green. For protein analyses, tissues were homogenized with the Qiagen TissueLyser II in 2% SDS lysis buffer supplemented with protease and phosphatase inhibitors. Protein concentration was measured by bicinchoninic protein assay. Proteins were then resolved on 12% SDS-PAGE. The protein gels were then transferred to polyvinylidene fluoride (PVDF) membranes. Blots were probed with target antibodies and visualized using the FluorChem imaging system. Images were quantified with densitometry using the AlphaView software.

2.6. Mitochondrial isolation

To isolate mitochondria for respirometry analyses, brown fat pads were isolated and mechanically disrupted with scissors in a hypotonic mitochondrial isolation buffer (300 mM sucrose, 5 mM HEPES, 1 mM EDTA, pH 7.2 with KOH). Minced brown adipose tissue was then lysed using a glass-Teflon homogenizer with a tight-fitting pestle using 15 strokes. Homogenates were filtered by 100 mM mesh filter and centrifuged at 600*g* to remove the nuclei and cellular debris. The supernatant was retained and centrifuged at 8,500*g* for 10 min to isolate mitochondria. Mitochondria were then resuspended in MAS buffer [40] (70 mM sucrose, 220 mM mannitol, 5 mM KH2PO4, 5 mM MgCl, 2 mM HEPES, 1 mM EGTA, pH7.2 with KOH) and quantified by bicinchoninic protein assay. To isolate mitochondria for WB analyses, the Qproteome Mitochondria Isolation Kit was used. For mitochondria protection assays, isolated and purified mitochondria were treated with or without proteinase K (10ug/ml) for 30min at RT.

2.7. Cellular and mitochondrial respiration assay

Oxygen consumption rate (OCR) was measured by Seahorse XFe24 analyzer (Agilent). For cellular respirometry analyses, primary brown adipocytes were differentiated in XFe24 cell culture plates as previously described. To assess cellular CL-induced respiration, cells were washed and switched to unbuffered DMEM supplemented with 4.5 g/L glucose, 4 mM glutamine, 100 mM pyruvate, and 2% of fatty acid-free BSA, pH7.4 by NaOH on day 7 post-differentiation. For cellular beta-oxidation test, cells were washed and switched to unbuffered DMEM supplemented with 0.5 mM glucose, 1 mM glutamine, 0.5 mM L-carnitine, 1% FBS for starvation for 24 h. On the day of the assay, cells were switched into unbuffered DMEM supplemented with 2 mM glucose, 0.5 mM L-carnitine, incubated for 30min and then put into the assay. The compounds concentrations were as follows (final concentration): For CL-driven respiration, Port A: CL 316, 243 (10 mM) and Port B: Rotenone/Antimycin A (4 μM each); for beta-oxidation test, Port A: Etomoxir (10 μM). Port B: Oligomycin (4.5 μM), Port C: DNP (0.6 mM), Port D: Rotenone/Antimycin A (4 μM each). For mitochondrial respirometry analyses, fresh mitochondria from interscapular brown adipose tissue were isolated as previously described. Then 5 μg of mitochondria were centrifuged from hypotonic isolation buffer and resuspended in 50 μl of MAS buffer per well in a seahorse plate. The seahorse plate was centrifuged at 2000g for 20min to adhere to the mitochondria. Then 450 μl of MAS buffer was carefully added to each well. The mitochondrial stress test compounds were as follows (final concentration): Palmitoyl-L-carnitine (50 μM) (for palmitate-driven respiration). Respirometry data were collected using the Agilent Wave software v2.4.

2.8. Body composition

Body composition to assess lean and fat mass were measured via NMR using the Minispec LF65 Body Composition Mice Analyzer (Bruker, Karlsruhe, Germany)

2.9. Mitochondrial and whole cell proteomics

To analyze the mitochondrial proteome, total mitochondria were isolated from brown fat tissue as described above. BAT mitochondria were isolated from 8-week-old male mice exposed to TN or Cold environment ($n = 3$ per group) and lysed in radio immunoprecipitation buffer (RIPA) [150 mM NaCl, 50 mM Tris-Cl pH 7.5, 0.5% NP-40, 0.1% Sodium deoxycholate, supplemented with protease and phosphatase inhibitors]. To analyze the whole cell proteome, brown adipose fat pads were isolated and lysed in 2% SDS solution supplemented with protease and phosphatase inhibitors. Sample lysates were quantified by bicinchoninic protein assay and delivered to the Biotechnology Resource Center (BRC) at Cornell University for Tandem Mass-Tagged (TMT) shotgun-based quantitative proteomics. Briefly, proteins were denatured, reduced, cysteine blocked, and digested using the S-trap approach. The resulting trypic peptides were TMT-labeled, and pooled. The labeled peptides were then fractionated by high pH reverse phase chromatography by the Ultimate 3000 MDLC platform into 10 fractions. Then samples were subjected to nanoLC-MS/MS analysis using a reverse phase HPLC separation and NanoLC RP coupled with an Orbitrap Eclipse mass spectrometer (Thermo Scientific) equipped with a nano ion source. Ion quantification and proteomic database searches were conducted using the Proteome Discoverer 2.4 software against the mouse database. All MS and MS/MS raw spectra were processed using Proteome Discoverer 2.4 (PD 2.4, Thermo) for reporter ion quantitation analysis. Statistics were calculated according to the Cold/TN mice in mitochondrial proteomics; and N1—KO/N1-Flox mice in the N1—KO mice BAT tissue proteomics; conducted by the proteomic core facility. Statistical test normalization and significance test information is detailed in the statistic section. Gene ontology was performed by EnrichR [41,42]. The mass spectrometry proteomics data have been deposited to the ProteomeXchange Consortium via the PRIDE partner

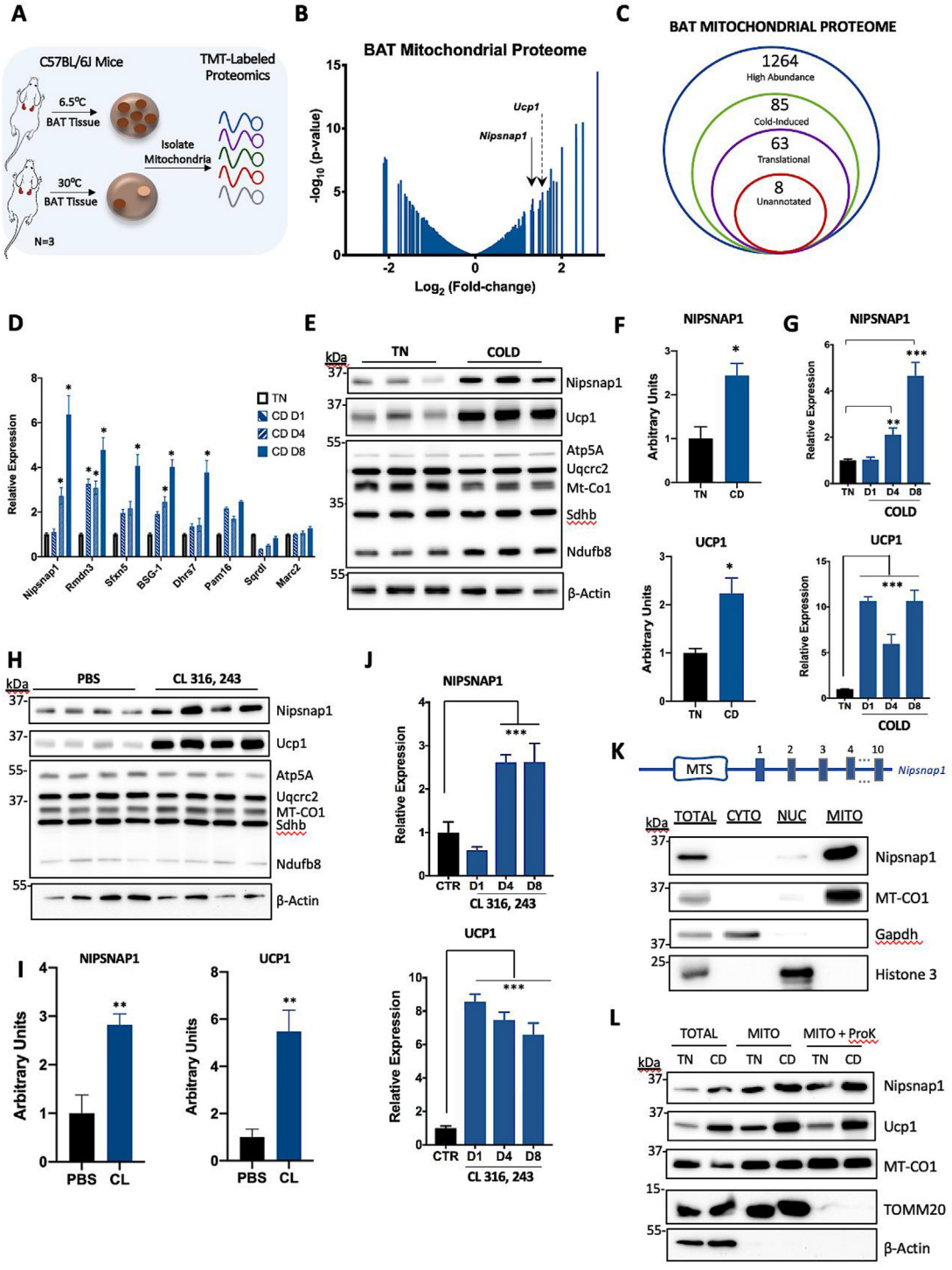

Figure 1: Nipsnap1 harbors late-stage thermogenic expression profile in BAT **(A)** Schematic of BAT mitochondrial proteomic analysis in chronic cold compared to TN-exposed wild-type (WT) male mice. **(B)** Line volcano plot of the mitochondrial proteins identified in BAT mitochondria (Cold vs TN, n = 3 per group). **(C)** Diagram of filtering process to identify unannotated mitochondrial proteins. **(D)** Relative mRNA expression from WT mice exposed to 1, 4, and 8 days of cold (CD) exposure compared to thermoneutral controls (n = 3). **(E)** Representative Western blot of BAT tissue from WT male mice exposed to TN and Cold for 8 days. **(F)** Densitometry of Nipsnap1 (above) and Ucp1 (below) protein levels normalized to β-Actin from Figure 1E. **(G)** Relative mRNA time-course expression of Nipsnap1 (above) and Ucp1 (below) from WT male mice exposed to 1, 4, 8 days of cold exposure compared to thermoneutral controls (n = 5). **(H)** Representative Western blot of BAT tissue from male mice treated with CL 316,243 or PBS IP injection for 8 days. **(I)** Densitometry of Nipsnap1 (left) and Ucp1 (right) protein levels normalized to β-Actin from Figure 1H. **(J)** Relative mRNA time-course expression of Nipsnap1 (above) and Ucp1 (below) from male mice treated with CL 316,243 or PBS IP injection for 1, 4, and 8 days compared to PBS-treated controls (n = 5). **(K)** Diagram of Nipsnap1 gene with the mitochondrial targeting sequence indicated (top); Representative Western blot for Nipsnap1 expression in different subcellular compartments from the BAT tissue of 10 day cold-exposed WT mice (bottom). **(L)** Mitochondrial protease protection assay on mitochondria isolated from the BAT tissue of 10 day cold-exposed male WT mice (bottom). qPCR data are represented as mean ± SEM. Significance is denoted as *p < 0.05, **p < 0.01 ***p < 0.001 by Student's t test.

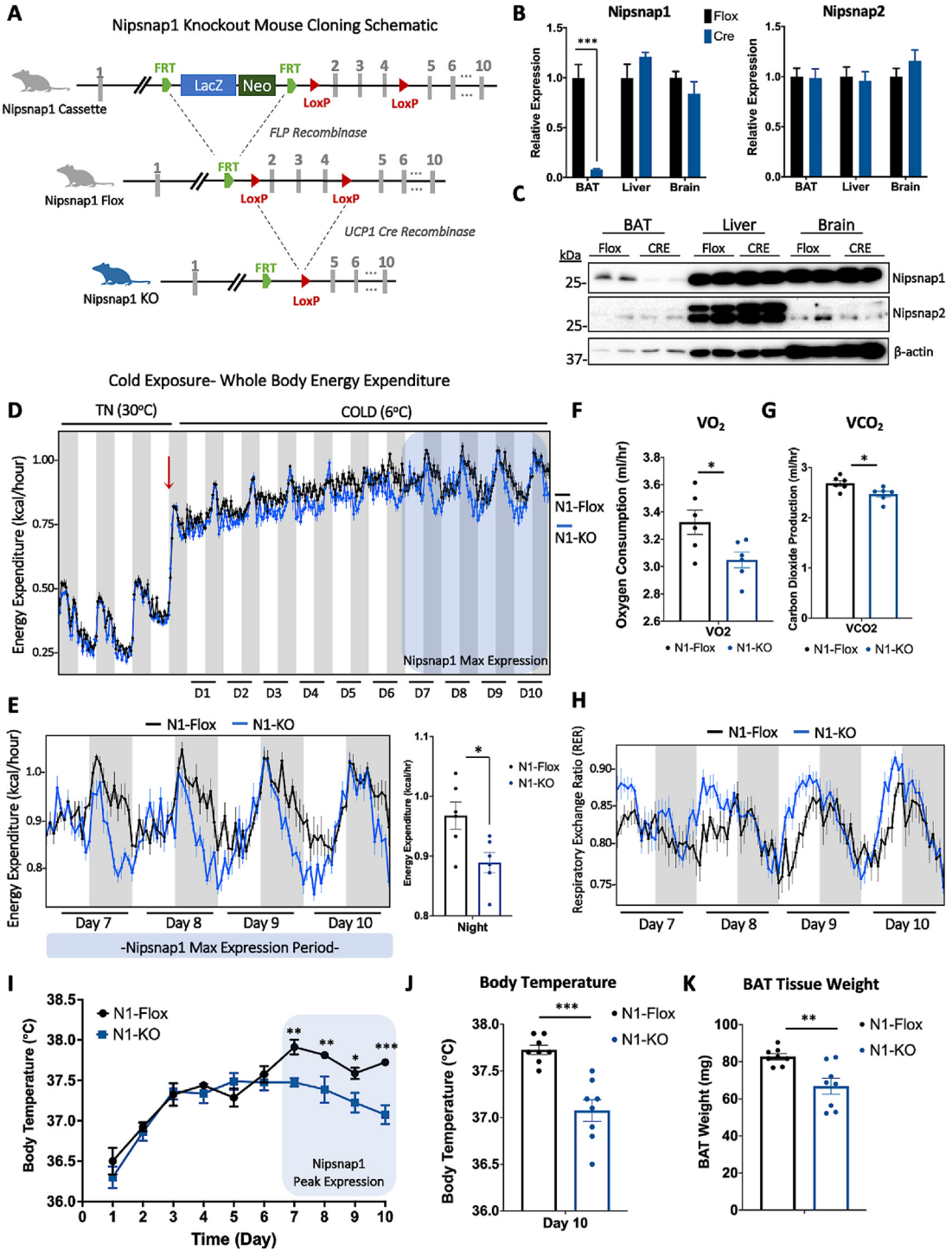

Figure 2: Nipsnap1 ablation in BAT causes severe defect in the maintenance phase of NST. **(A)** Diagram of breeding strategy to generate conditional Nipsnap1 knockout mouse in thermogenic adipose tissue. **(B)** Relative Nipsnap1 and Nipsnap2 mRNA expression in prolonged cold-induced N1-Flox and N1−KO mice in BAT, Liver, and Brain tissue (n = 5). **(C)** Representative Western blot for Nipsnap1 and Nipsnap2 from prolonged cold-induced N1-Flox and N1−KO mice. **(D)** Energy expenditure of male N1-Flox and N1−KO mice exposed to thermoneutral (TN, 30 °C) for 3 days followed by prolonged cold (COLD, 6 °C, red arrow) for 10 days (n = 6). Grey bars denote the dark cycle and white bars indicates the light cycle. Blue shaded region indicates an overlay of Nipsnap1 maximal expression period. Red arrow indicates the switch to cold temperatures **(E)** Zoomed-in diagram of energy expenditure plot (from the blue shaded region from 2D) of male N1-Flox and N1−KO mice representing day 7−10 of cold exposure (COLD, 6 °C). Quantification is indicated to the right. **(F)** Oxygen consumption of male N1-Flox and N1−KO (n = 6) mice at cold-exposed day 7−10 (n = 6). **(G)** Carbon dioxide production of male N1-Flox and N1−KO (n = 6) mice at cold-exposed day 7−10. **(H)** Respiratory exchange ratio (RER) measurement of male N1-Flox and N1−KO (n = 6) mice on day 7−10 exposed to cold (COLD, 6 °C) **(I)** Daily rectal temperature measurement of male N1-Flox and N1−KO exposed to cold (COLD, 6 °C) for 10 days (n = 8). **(J)** Quantification of Figure 2I (K) BAT tissue weight from male N1-Flox and N1−KO mice exposed to cold for 10 days (n = 8). Whole body metabolic assessments (D and E) were analyzed by ANCOVA. All other figures unless otherwise indicated are data represented as mean ± SEM. *p < 0.05, **p < 0.01 ***p < 0.001 by Student's t test.

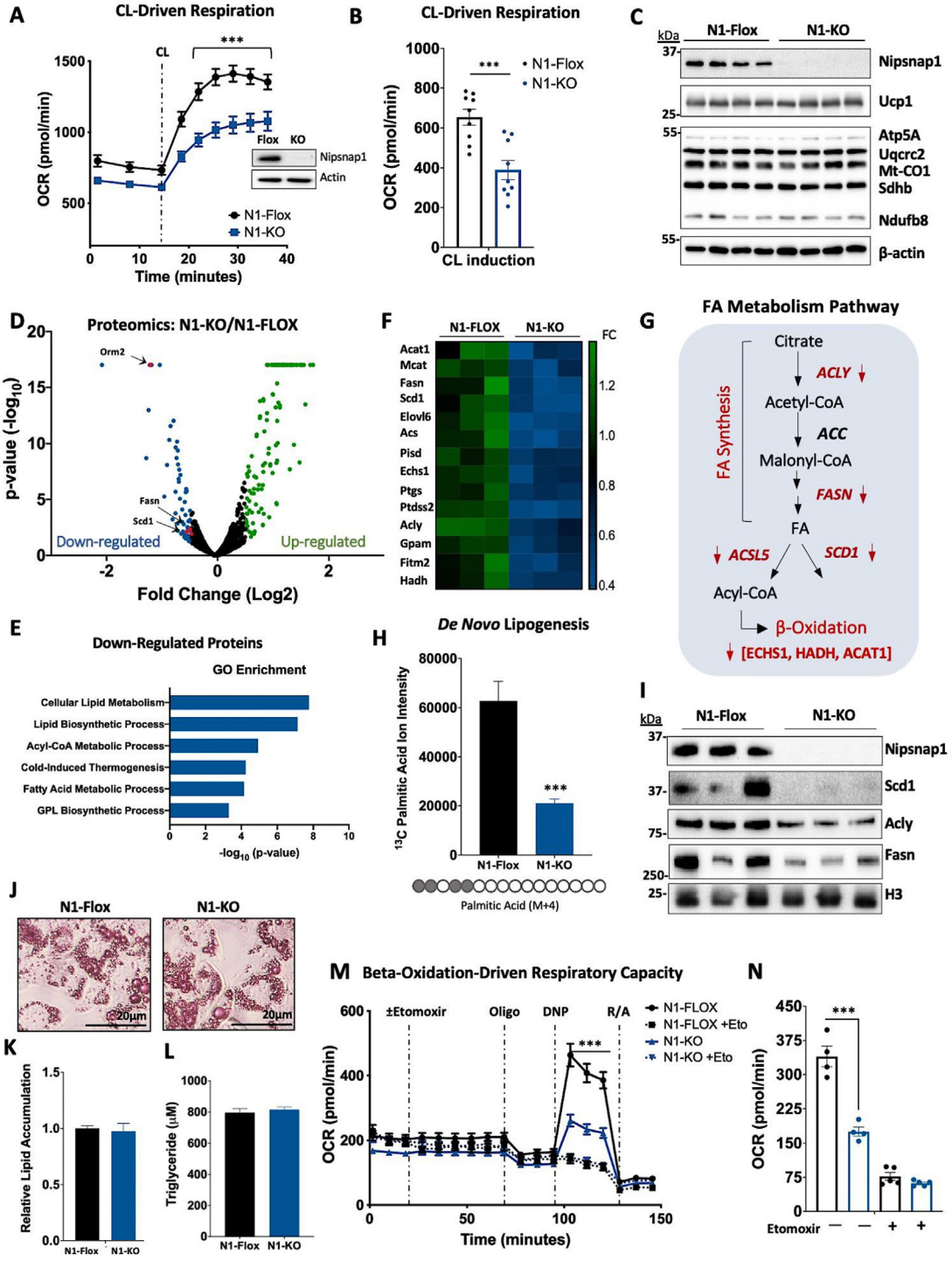

Figure 3: Ablation of Nipsnap1 leads to severe defects in BAT Lipid Metabolism. **(A)** Oxygen consumption rate of N1-Flox and N1−KO primary brown adipocytes (n = 10). CL, CL 316, 243; The western blot inlay represents deletion of Nipsnap1 **(B)** Quantification CL-induced oxygen consumption rate from 3 A of N1-Flox and N1−KO primary brown adipocytes with antimycin/rotenone and basal OCR values subtracted to represent true mitochondrial respiration (n = 10). **(C)** Representative Western blot of BAT from 10-day cold-induced N1-Flox and N1−KO female mice. **(D)** Volcano plot of the proteins upregulated (green) and downregulated (blue) from the BAT tissue proteomic analysis of female N1−KO mice compared to N1-Flox controls after 10-day cold exposure. **(E)** Gene ontology analysis of the down-regulated proteins from female N1−KO BAT proteome compared to N1-Flox BAT in 10-day cold exposure. **(F)** Heatmap representing the lipid metabolic genes that were downregulated in N1−KO BAT compared to N1-Flox after 10 days of cold exposure. **(G)** Diagram depicting the down-regulated proteins in the lipid metabolic pathway. **(H)** ^{13}C labeled palmitic acid from N1-Flox and N1−KO primary brown adipocytes as a proxy for *de novo* lipogenesis. **(I)** Representative Western blot validating select down-regulated proteins involved in lipid metabolism in BAT from N1−KO and N1-Flox female mice after 10 days of cold exposure. **(J)** Representative Oil red O staining image of differentiated N1-Flox and N1−KO primary brown adipocytes. **(K)** Quantification of Oil red O staining from **(J)** (n = 3). **(L)** Total triglyceride levels in N1-Flox and N1−KO brown adipocytes (n = 5). **(M)** Beta-oxidation-driven respiratory capacity with the Seahorse Bioanalyzer in the N1-Flox and N1−KO primary brown adipocytes (n = 5). **(N)** Quantification of beta-oxidation-driven basal oxygen consumption rate of N1-Flox and N1−KO primary brown adipocytes (n = 5). All Seahorse data and palmitic acid measurements are represented as mean ± SEM. *p < 0.05, **p < 0.01 ***p < 0.001 by Student's t test.

repository with the dataset identifiers PXD043251 (Mitochondrial proteomics-Figure 1B) and PXD043252 (N1—KO vs N1-Flox proteomics- Figure 3D).

2.10. Oil Red O staining

Oil red O staining was performed as described previously [43]. In short, Oil Red O stock solution was prepared by dissolving 0.2 g Oil red O powder in 40 ml isopropanol. A 2:3 stock to distilled water working solution was then prepared and filtered immediately before use. For cell staining, cells were washed with PBS and fixed in 4% formaldehyde in PBS for 15min at RT. Fixed cells were then washed 3 times with PBS, and Oil red O working solution was then added. After 30min incubation with mild shaking at RT, cells were washed 5 times in PBS and then imaged with an Olympus IX71 Inverted Fluorescence Microscope. Images were acquired and analyzed by OLYMPUS cellSens Entry 3.2. For staining quantification, 1 ml isopropanol was added to the stained cells. The plate was incubated for 10min at RT with mild shaking. 200 μl of the eluate per sample was then transferred to a clear bottom 96-well plate along with 200 μl pure isopropanol as a blank control. Absorption was measured at 510 nm by SpectraMax M3 and data was acquired and interpreted by SoftMax Pro 6.

2.11. Measurement of cellular triglycerides

Mouse primary brown adipocytes were seeded on a 96-well plate and differentiated as described in Method 2.2. Total triglycerides were measured using Triglyceride-Glo™ Assay (Promega J3160) following the manufacturer's instructions.

2.12. *De novo* lipogenesis stable isotope tracing of free fatty acids

Mouse primary brown adipocytes were harvested, cultured, and differentiated as described previously. After 6 days in maintenance media, primary cells were washed twice with pre-warmed PBS, then incubated with glucose-free DMEM media supplied with 25 mM ^{13}C-Glucose and 4 mM Glutamine, pH7.4 for 4hrs. At the end of incubation, primary cells were washed three times with PBS, then free fatty acids were extracted from cells using 90% methanol (LC/MS grade, Thermo Scientific A456-500). The extracts were clarified by centrifugation at 14,000 g for 20 min at room temperature. The supernatants were collected and sent to the Proteomics and Metabolomics Core Facility at Weill Cornell Medicine, where samples were dried down using a SpeedVac. The dried sample was reconstituted using 50% methanol prior to LC-MS analysis. Chromatographic separation was performed on a Vanquish UHPLC system (Thermo Scientific) with a Cadenza CD-C18 3 μm packing column (Imtakt, 2.1 mm id x 150 mm) coupled to a Q Exactive Orbitrap mass spectrometer (Thermo Scientific) via an Ion Max ion source with a HESI II probe (Thermo Scientific). The mobile phase consisted of buffer A: 5 mM ammonium acetate in water (LC/MS grade, Thermo Scientific) and buffer B: 5 mM ammonium acetate, 85% isopropanol (LC/MS grade, Thermo Scientific), 10% acetonitrile (LC/MS grade, Thermo Scientific), and 5% water. The LC gradient was as follows: 0—1.5 min, 50% buffer B; 1.5—3 min, 50—90% buffer B; 3—5.5 min, 90—95% buffer B; 5.5—10 min, 95% buffer B, followed by 5 min of re-equilibration of the column before the next run. The flow rate was 150 μL/min. MS data was acquired in negative mode. The following electrospray parameters were used: spray voltage 3.0 kV, heated capillary temperature 350 °C, HESI probe temperature 350 °C, sheath gas, 35 units; auxiliary gas 10 units. For MS scans: mass scan range, 140—1000 *m/z*; resolution, 70,000 (at *m/z* 200); automatic gain control target, 1e6; maximum injection time, 50 ms. MS data files were processed using El-MAVEN (v0.12.0). Identification of free fatty acids and their 13C isotopologues was based on accurate masses within 5 ppm and standard retention times. Relative quantitation was performed based on MS signal intensities. The raw files for the lipidomics experiment (Figure 3H) has been uploaded to the Mendeley Data Repository can be found at the following link: https://data.mendeley.com/datasets/r8gymtsnrp/1.

2.13. Statistical analyses

Statistical analyses were calculated using GraphPad Prism 8 software in consultation with the Cornell Statistical Consulting Unit (CSCU). Specific statistical tests are indicated in each figure and most data are represented as the mean ± S.E.M unless otherwise indicated. Both unpaired two-tailed Student's T-test and two-way ANOVA were used with post hoc analysis by Bonferroni. For proteomic analysis, statistical analyses were conducted by the Biotechnology Resource Center (BRC). Briefly, target peptide signals were normalized by total peptide amount and the P-value was calculated by student's t-test with no correction for multiple testing using the Proteome Discoverer 2.4 software. Murine food consumption analysis was performed by ANCOVA using the CalR application and as described previously (Nature Methods 2012/ Muller et al. Nature Metabolism 2021 by ANCOVA, CalR website). At least two biological replicates were conducted for most *ex vivo* studies with independently derived primary cells. For animal experiments, an $n = 5—10$ per group for an alpha value of 0.05 and an effect size of >10—20% respectively was determined to yield significance. A minimum of 2 biological and/or technical replicates were performed for all *in vivo* experiments with appropriate vehicle controls.

3. RESULTS

3.1. Nipsnap1 harbors a late-stage thermogenic expression profile in BAT

To identify proteins that have the potential to serve as key mediators of late-stage thermogenic maintenance, we isolated mitochondria from interscapular BAT of mice exposed to either a chronic cold (6.5 °C) or a thermoneutral (30 °C) environment for 8 days and performed TMT-labeled proteomics (Figure 1A,B). Of the captured mitoproteome, protein candidates were subsequently filtered based on protein abundance in BAT (>100 copies), fold change response to cold induction (Cold/TN > 1.5 fold), orthologous expression to humans for translational potential (Expressed in human BAT proteome [44]), and novelty [41,42]) (Figure 1C). This yielded eight proteins as potential candidates. Of these candidates, Nipsnap1 emerged as the most significant based on protein and gene abundance levels in response to an 8-day chronic thermogenic activation (Figure 1D). Nipsnap1 protein induction was then confirmed by western blot, displaying a significant increase in BAT exposed to chronic cold conditions similar to UCP1—the classical marker of thermogenic activation, indicating that the Nipsnap1 may harbor thermogenic properties (Figure 1E,F). The increase in Nipsnap1 under chronic cold conditions was specific to only BAT, as there was no increase in inguinal white adipose tissue (iWAT) or in other tissues such as the brain and liver that are reported to have high expression of Nipsnap1 [33]. Moreover, there was also no increase in Nipsnap2, which shares strong homology with Nipsnap1 (Figure. S1E).

To map the expression dynamics of Nipsnap1 in BAT, we measured the protein and mRNA expression of Nipsnap1 at 1, 4, and 8 days representing acute, intermediate, and prolonged murine cold challenge conditions. Intriguingly, Nipsnap1 mRNA and protein induction did not begin until day 4 of cold exposure, unlike that of Ucp1 mRNA and protein levels that are robustly induced after just 1 day of cold exposure

(Figure 1G and Figure. S1F). This suggests that Nipsnap1 may play a role in the maintenance, rather than the initiation, of non-shivering thermogenesis. Similar induction and expression dynamics of Nipsnap1 was observed in pharmacologically activated non-shivering thermogenesis using the β3 receptor agonist CL 316, 243 (Figure 1H–J), which indicates that Nipsnap1 is regulated, at least in part, through the classical cAMP pathway that induces many other thermogenic genes. Nipsnap1 contains a mitochondrial-targeting sequence and has been shown to localize to the mitochondrial matrix in brain and liver previously [30]. To reveal the localization of Nipsnap1 in BAT, we fractionated BAT from chronic 10-day cold-exposed wildtype mice and probed cytoplasmic, nuclear, and mitochondrial compartments for Nipsnap1 expression. Indeed, Nipsnap1 was localized to the mitochondrial compartment in BAT (Figure 1K) and is located in the inner mitochondria as shown by mitochondrial protease protection assay (Figure 1L). Taken together, Nipsnap1 is a mitochondrial protein that exhibits a late-stage activation expression pattern in response to cold and β3 adrenergic stimuli suggesting that it may play a role in the maintenance of non-shivering thermogenesis rather than its activation.

3.2. Mice lacking Nipsnap1 in brown adipose tissue can no longer maintain effective non-shivering thermogenesis

To determine if Nipsnap1 plays a role in the maintenance of non-shivering thermogenesis in BAT, we generated a conditional Nipsnap1 knockout (KO) mouse in thermogenic adipose tissue termed N1–KO (Figure 2A). The N1–KO mice are fertile and viable with no obvious developmental defects. We confirmed that Nipsnap1 gene and protein levels were successfully reduced in BAT while remaining unchanged in liver and brain. Importantly, the expression of Nipsnap2, a close homolog of Nipsnap1, was unaffected in N1–KO mice (Figure 2B,C). To determine if Nipsnap1 is required for long-term thermogenic maintenance, we placed N1–KO and N1-Flox control mice in metabolic cages to analyze whole-body metabolism. Mice were acclimated in the metabolic cages for 3 days at thermoneutral (TN) temperature conditions (30 °C) before subsequent exposure to a 10-day chronic cold challenge. As expected, the shift from TN to cold temperatures resulted in a boost in energy expenditure, but we observed no significant differences between the N1-Flox control and N1–KO mice under TN conditions or in the early stages of cold exposure (thermogenic activation). Remarkably, however, a significant decline in whole-body energy expenditure emerged after 7 days of prolonged cold exposure (the thermogenic maintenance stage), which strikingly aligned with the period of maximum Nipsnap1 expression (day 7–10). Notably, these defects occurred during the night cycle when the mice are the most active (Figure 2D,E). The impaired energy expenditure persisted despite no differences in total food consumption and locomotor activity between the N1–KO mice and the N1-Flox controls (Figures. S2A and S2B). Significant defects were also observed in VO_2 and VCO_2 levels during prolonged cold challenge conditions with no changes in overall energy balance (Figure 2F,G and Figures. S2C–S2G). Furthermore, the N1–KO mice displayed an elevated respiratory exchange ratio revealing a metabolic shift from lipid to carbohydrate metabolism, suggesting a potential defect in the ability to metabolize lipids (Figure 2H and Figure. S2H). To determine if the defect in energy expenditure observed during the late-stage thermogenic maintenance period in the N1–KO mice translated to disordered whole-body thermoregulation—a proxy for BAT function, we assessed daily body temperature of N1–KO mice compared to N1-Flox controls under chronic cold conditions for 14 days. Consistent with what was observed previously with energy expenditure, the N1–KO and N1-Flox mice were both able to successfully protect their body temperature against cold in the early stages of thermogenesis. However interestingly, N1–KO mice began to exhibit defects in thermoregulation at day 7 which aligns with the Nipsnap1 maximal expression period (Figure 2I,J). Tissue level analysis revealed that the BAT and IWAT in N1–KO mice displayed a significant decrease in tissue weight compared to N1-Flox controls while the eWAT depot was unaffected (Figure 2K and Figure. S2I). No differences in overall body weight, fat, or lean mass were observed (Figure. S2J-S2L). Taken together, Nipsnap1 ablation in BAT leads to an impaired ability to sustain thermogenic activation. N1–KO mice, when compared to N1-Flox controls, are initially able to protect their body temperature when faced with a cold challenge through an active thermogenic process, but later display a defect in their ability to maintain effective thermogenesis due to their inability to express Nipsnap1.

3.3. Ablation of Nipsnap1 leads to defects in BAT lipid metabolism

Given the inability of the Nipsnap1 knockout mice to sustain long-term activation of thermogenesis and their corresponding decline in whole-body energy expenditure, we interrogated whether the defects in thermogenesis originate specifically from brown fat. We therefore isolated and cultured primary N1-Flox and N1–KO brown adipocytes and assessed cellular respirometry using the Seahorse Bioanalyzer. Indeed, significant defects in cellular respiration were observed in N1–KO adipocytes, impacting both basal and CL-induced oxygen consumption rates (Figure 3A,B). Based on these results and the known defects in thermogenic maintenance and energy metabolism *in vivo*, we hypothesized that Nipsnap1 deficiency could be compromising classical UCP1-dependent thermogenesis. To test this, we performed thermogenic protein and gene profiling in BAT. Surprisingly, there were no differences in classical thermogenic markers or core mitochondrial genes at either the protein or RNA level (Figure 3C and Figures. S3A–S3C). To gain mechanistic insight as to how the ablation of Nipsnap1 could be causing such drastic defects in the maintenance of non-shivering thermogenesis, we performed TMT-labeled proteomics in the brown adipose tissue of our N1–KO mice compared to N1-Flox controls exposed to chronic cold conditions for 10 days to interrogate proteome changes during the thermogenic maintenance phase. We observed a host of significantly differentially expressed proteins and subsequent gene ontology analyses revealed that the majority of the down-regulated proteins were associated with lipid metabolism processes (Figure 3D,E). Indeed, many core lipid metabolism proteins such as ATP Citrate Lyase (Acly), Fatty Acid Synthase (Fasn), and Stearoyl CoA Desaturase (Scd1) were significantly reduced in N1–KO mice compared to N1-Flox controls (Figure 3F–G). Curiously, there were no changes at the mRNA level for lipid metabolism genes, which indicates a potential role for Nipsnap1 in the post-translational regulation of lipid metabolism proteins (Figure. S3D). Given these significant changes in lipid metabolism protein levels, we postulated that either *de novo* lipogenesis (DNL), lipid accumulation, lipid signaling capacity, and/or lipid beta-oxidation may be impacted. In order to determine if ablation of Nipsnap1 in BAT led to defects in DNL, we cultured primary N1–KO and N1-Flox brown adipocytes in the presence of high concentrations of ^{13}C labeled glucose to initiate DNL. We then measured the incorporation of ^{13}C carbons into free fatty acids. N1–KO brown adipocytes had significantly lower levels of ^{13}C carbon incorporation into palmitic acid and other free fatty acids compared to N1-Flox controls suggesting significant impairments in DNL (Figure 3H and Figures. S3E and S3F). Indeed, Fasn, Acly, and Scd1 protein levels which are key players in DNL were significantly reduced via immunoblot analysis (Figure 3I). Curiously, ablation of Nipsnap1 did not alter

lipid storage capacity, as measured by Oil Red O staining, or total triglycerides levels in primary N1—KO brown adipocytes compared to N1-Flox controls (Figure 3J-L). We next examined whether loss-of-Nipsnap1 conferred defects in key lipid proteins in response to norepinephrine (NE) signaling. To test this, we interrogated levels of phosphorylated hormone-sensitive lipase and phosphorylated acetyl CoA carboxylase in primary brown adipocytes from N1—KO and N1-Flox mice exposed to NE. We noted no differences in lipid signaling in response to acute NE treatment (Figure. S3G). Finally, we wanted to assess whether functional beta-oxidation capacity was affected. We therefore performed cellular respirometry analyses in primary N1-Flox and N1—KO brown adipocytes in the presence or absence of the carnitine palmitoyl transferase 1 (CPT1) inhibitor etomoxir which inhibits fatty acid oxidation [45,46]. To trigger cellular beta-oxidation, we exposed fully differentiated N1-Flox and N1—KO brown adipocytes to a starvation media containing 0.5 mM glucose, 1 mM glutamine, and 0.5 mM L-carnitine for 12 h to deplete glucose levels and force the brown adipocytes to use their intrinsic lipid stores as the primary substrate for energy. We then performed cellular respirometry analysis to evaluate beta-oxidation capacity. We observed severe defects in the DNP-induced maximal respiratory capacity of N1—KO primary brown adipocytes compared with N1-Flox controls (Figure 3M,N). The impaired beta-oxidation capacity in primary brown adipocytes prompted us to assess whether these defects in fatty acid metabolism were also present *in vivo*. To test this, we isolated BAT mitochondria from mice that were chronically exposed to a 10-day cold temperature challenge and performed palmitate-driven respirometry analyses in isolated mitochondria from N1—KO mice compared to N1-Flox controls. Remarkably, there was also a defect in beta-oxidation capacity present in isolated chronically cold-activated mitochondria from N1—KO mice compared to N1-Flox controls (Figures. S3H—S3I). This defect in mitochondrial beta-oxidation capacity mechanistically supports our earlier findings in which we observed a macronutrient metabolism shift in N1—KO mice to favor carbohydrate metabolism over the oxidation of lipids due to impaired lipid metabolism (Figure 2H). Taken together, the significant defects in lipid beta-oxidation capacity observed in both isolated mitochondria from BAT tissues, as well as in primary brown adipocytes from N1—KO mice compared to N1-Flox controls mechanistically contributes to the inability to sustain effective non-shivering thermogenesis when faced with a chronic cold challenge. This is further compounded by defects in DNL which may decrease endogenous lipid substrate availability for cellular oxidation. These results suggest that Nipsnap1 integrates with lipid metabolism and when ablated in BAT, leads to significant declines in DNL and beta-oxidation capacity.

3.4. Nipsnap1 KO mice activate a hyperphagic response to pharmacological β3 activation with CL 316, 243

Given that our findings strongly point towards an integrated role of Nipsnap1 with beta-oxidation capacity (Figure 3J-L), we hypothesized that pharmacological activation of NST *in vivo* would be severely impacted as this process heavily relies on functional beta-oxidation. We therefore placed 8-week-old N1—KO mice and N1-Flox controls in the Promethion metabolic cages and administered daily intraperitoneal injections of the β3 agonist CL 316, 243 under TN environmental conditions for 10 days. On the first day following CL injection, we observed the expected boost in energy expenditure in response to CL administration similarly between the N1-Flox control and N1—KO groups (Figure 4A). Surprisingly however, as daily CL administration continued over the course of 10 days, we did not observe any differences between the N1-Flox control and N1—KO groups in energy expenditure, VO_2, or VCO_2 during the late-stage thermogenic maintenance phase (Figure 4B and Figures. S4A—S4D). There were also no differences between the levels of lipid metabolism proteins, total body weight, or adipose tissue depots although the BAT tissue weight trended lower in the N1—KO mice compared to controls (Figure 4C—E). This was stark contrast to the significant defects in VO_2 and VCO_2 levels observed when the N1—KO mice were exposed to cold environmental conditions. We then speculated whether a compensatory mechanism was taking place with upon pharmacological β3 NST stimulation to promote the normalization of the energy expenditure levels in the N1—KO mice to match the N1-Flox controls. Intriguingly we observed a significant increase in food consumption in N1—KO mice compared to N1-Flox controls during the CL-driven thermogenic maintenance phase (Day 7—10) when Nipsnap1 is maximally expressed (Figure 4F). This hyperphagic response in the N1—KO mice led to a positive energy balance compared to N1-Flox controls that was only significant in the thermogenic maintenance phase (Figure 4G,H). Given that the increase in food consumption was not coupled to differences in body weight or significant locomotive movement (Figure. S4E), it is plausible that this contributed instead to increasing VO_2 and VCO_2 thereby normalizing energy expenditure levels in the N1—KO mice to that of the N1-Flox controls. Taken together, CL-stimulated NST activation under TN conditions in the N1—KO mice triggers a hyperphagic response that is only seen in the NST maintenance period when Nipsnap1 is maximally expressed. The increase in food consumption, uncoupled to a change in body weight or locomotive movement, may be a driver for the normalization of energy expenditure in the N1—KO mice compared to N1-Flox controls.

3.5. Nipsnap1 KO mice do not have increased susceptibility to diet-induced obesity

To determine if the BAT-specific ablation of Nipsnap1 would render N1—KO mice more susceptible to diet-induced obesity, we challenged the N1—KO mice and N1-Flox controls with a high fat diet (HFD) or a chow feeding regimen under thermoneutral conditions for 24 weeks. As expected, the HFD feeding led to a significant weight gain in both N1-Flox and N1—KO mice compared to the chow fed groups, but there were no differences between genotypes (Figure 5A). We postulated that perhaps there were no differences in weight gain because Nipsnap1 levels are minimally expressed under thermoneutral environmental conditions. Indeed, though we observed a mild increase in Nipsnap1 levels due to diet-induced-obesity in the N1-Flox mice, the increase in Nipsnap1 protein levels is not as potent as what is observed under cold exposure conditions (Figure 5B). Therefore, we interrogated the response to HFD, but this time, under constant cold-exposure conditions for 24 weeks in which Nipsnap1 would be robustly expressed. We monitored weight gain throughout the duration of the study and though the mice did not experience as much weight gain under cold-exposed conditions when paired with a HFD compared to mice in thermoneutral conditions, there remained no differences in weight gain between the N1-Flox and N1—KO groups (Figure 5A,C). To assess if Nipsnap1 played a regulatory role in whole-body glucose metabolism in response to a cold-exposed high fat diet, we performed glucose and insulin tolerance tests (GTT and ITT respectively). There were no differences in GTT or ITT between N1-Flox and N1—KO groups (Figure 5D,E). There were also no differences in body composition, or in adipose depots weights after HFD feeding in a cold environment (Figure 5F, G, and Figure. S5A). Lastly, we noted no alterations of Nipsnap2 expression levels between N1-Flox and N1—KO mice (Figure. S5B). To determine if the defects with lipid metabolism that was observed under chow fed cold-exposure conditions persisted to

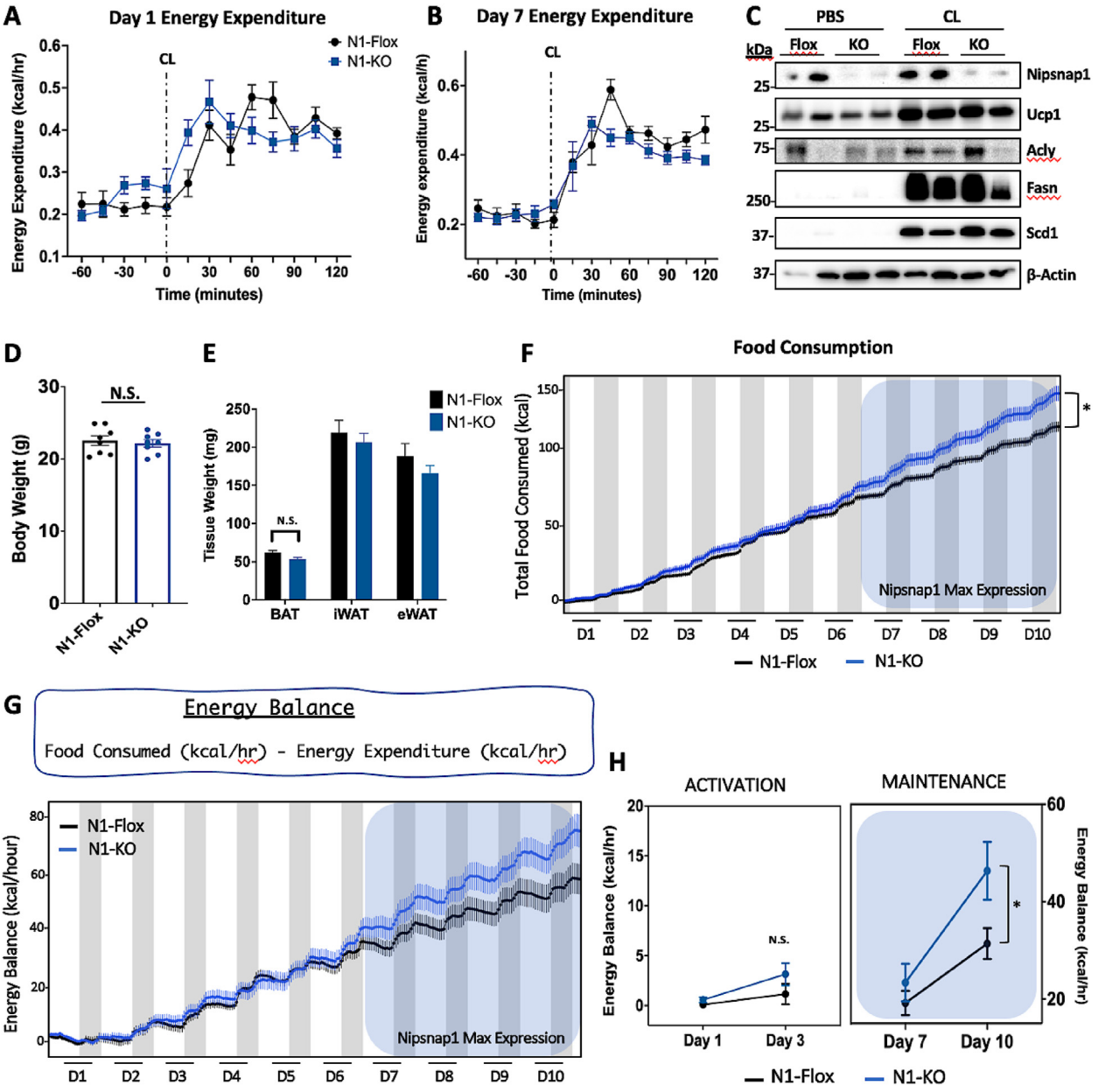

Figure 4: Nipsnap1 KO Mice trigger a hyperphagic response to pharmacological β3 activation with CL 316, 243 in TN conditions. (**A-B)** Energy expenditure at day 1 and day 7 of male N1-Flox and N1−KO mice injected daily with CL 316, 243 at thermo-neutral (TN, 30 °C, n = 7). Dotted line indicates the time point of CL injection. **(C)** Representative Western blot of BAT from male N1−KO and N1-Flox mice that were injected with daily CL or PBS injection at thermoneutrality for 10 days (TN, 30 °C, n = 7). **(D−E)** Body weight and tissue weight of male N1-Flox and N1−KO mice daily injected with CL 316, 243 under the thermoneutral conditions for 10 days (n = 7). **(F)** Accumulated food consumption of male N1-Flox and N1−KO mice injected daily with CL 316, 243 under the thermoneutral condition for 10 days (n = 7). **(G)** Top, equation to calculate Energy Balance by the CalR analysis program; Bottom, Accumulated Energy Balance of male N1-Flox and N1−KO mice injected daily with CL 316, 243 under thermo-neutral conditions (TN, 30 °C) for 10 days (n = 7) in the Promethion metabolic cages. **(H)** Quantification of Energy Balance change during NST activation (Day 1−3) and NST maintenance (Day 7−10). Accumulated Food Consumption **(F)** was analyzed by ANCOVA; All other figures unless otherwise indicated are data represented as mean ± SEM. *p < 0.05 by Student's t test.

cold-exposed HFD feeding, we profiled selected thermogenic and lipid metabolism genes. Thermogenic genes and proteins were unaltered as observed previously, but unlike the impaired lipid metabolism signatures that were seen under chronic cold chow-fed diet conditions, we no longer noted any significant defects in target lipid metabolism proteins such as Acly and Scd1 (Figures 3G and 5H, and Figures. S5D−S5F). Taken together, we conclude that ablation of Nipsnap1 in the brown fat of chow fed animals results in significant defects in the cold-induced maintenance of non-shivering thermogenesis due to a defect in lipid metabolism. It appears however that when mice are switched to a HFD under cold conditions they do not experience excessive weight gain compared to N1-Flox controls. We hypothesize that the increased nutrient density and lipid availability from the high fat diet feeding may normalize the lipid metabolism in beta-oxidation defects seen previously and provide sufficient substrates for the mitochondria to protect against excessive weight gain.

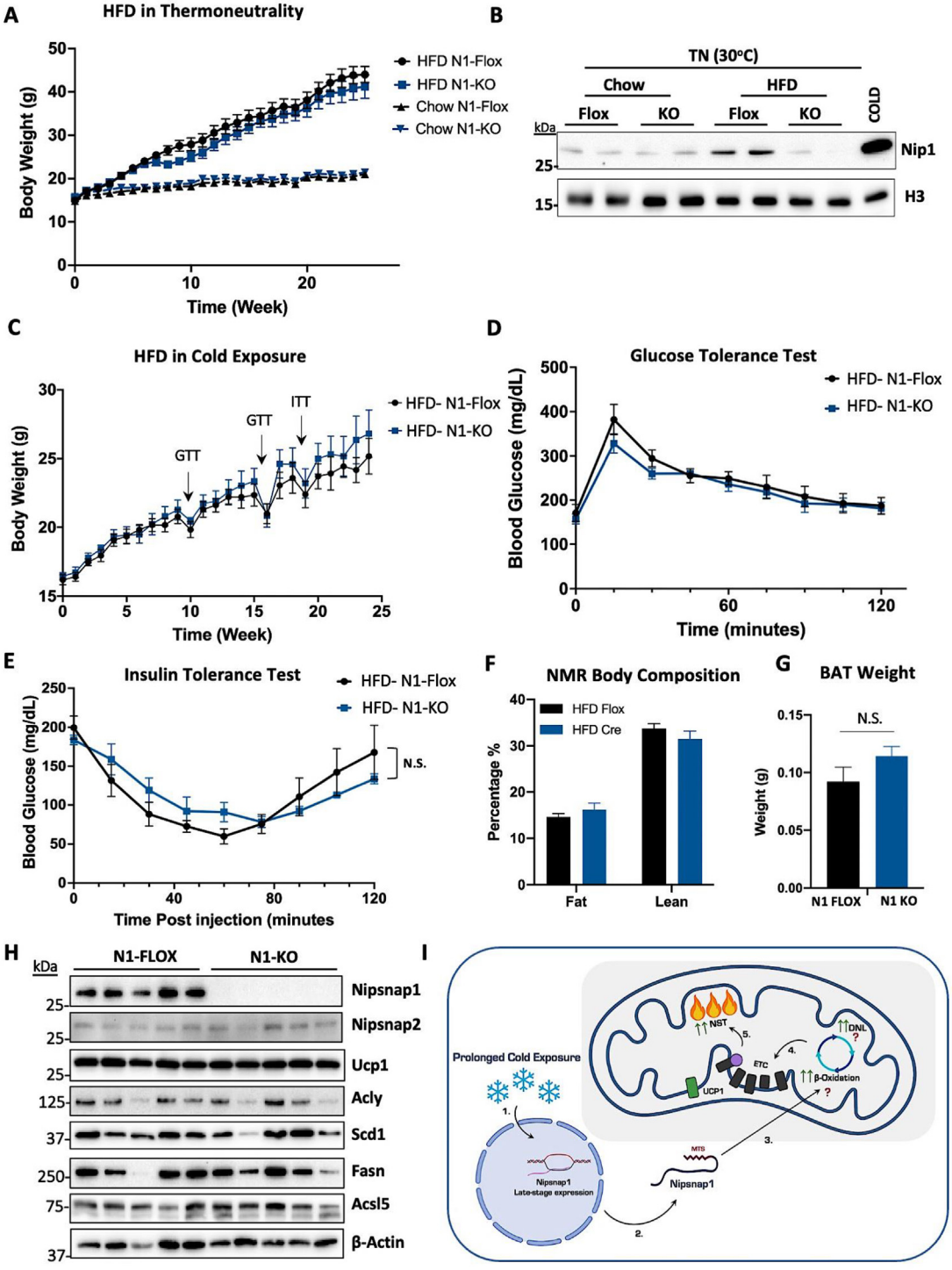

Figure 5: Nipsnap1 KO mice do not have increased susceptibility to DIO (A-B) Bodyweight measurement and BAT representative Western blot for high fat diet fed female N1-Flox and N1−KO mice in thermoneutral condition for 24 weeks (n = 10). Cold sample in **(B)** represents BAT lysate from a N1-Flox female mouse exposed to cold for 10 days as a control. **(C−H)** Bodyweight measurement, GTT, ITT, Body Composition, BAT tissue weight, and representative Western blot for high fat diet fed female N1-Flox and N1−KO mice in Cold (6 °C) for 24 weeks (n = 5). **(I)** Mechanistic diagram depicting the model of how Nipsnap1 interfaces with lipid metabolism to maintain long-term non-shivering thermogenesis. MTS- mitochondrial targeting signal, DNL-*de novo* lipogenesis, NST-non shivering thermogenesis, ETC- electron transport chain. All data represent mean ± S.E.M. Statistics were performed using Student's T test. N.S- Not significant.

4. DISCUSSION

Targeting brown adipose tissue in order to activate non-shivering thermogenesis and increase energy expenditure has been studied for decades [47,48]. To date, the field has made some outstanding advances to identify novel pathways such as succinate metabolism, and futile creatine cycling, in addition to many others that can be targeted to safely activate this protective metabolic process [49—52]. Despite these advances, however, the BAT-mediated increase in energy expenditure in both human and rodent models only persists when BAT is in its activated state [53,54]. BAT activation is known to be temporal, so once the activation stimulus, such as cold exposure, is removed, BAT is rapidly deactivated within hours and all protection is lost. The mechanisms surrounding how BAT maintains thermogenic function once initially activated, or the regulatory factors involved with the BAT maintenance process are relatively unexplored and represent a critical knowledge gap in the field.

Here we have identified Nipsnap1 that displays potent late-stage thermogenic properties in response to both cold environmental exposure and pharmacological β3-adrenergic activation. Nipsnap1 exhibits a late-stage thermogenic response that makes it suitable for consideration as a potential thermogenic maintenance factor instead of a novel candidate involved in NST activation. Indeed, the Nipsnap1 KO mice were fully capable of activating the thermogenic program in response to environmental or pharmacological challenges, but then later fail to sustain this activation in the maintenance stage of thermogenesis. Furthermore, the timing of the decline in VO_2 and VCO_2 respiratory capacities in the N1—KO mice compared to N1-Flox controls aligned perfectly with the Nipsnap1 expression dynamics. This mechanistically supports the findings that N1-Flox control mice with ample amounts of Nipsnap1 are able to switch seamlessly from thermogenic activation to the thermogenic maintenance phase, whereas the Nipsnap1 KO mice failed to effectively transition to the maintenance stage and were not able to retain the benefit of the initial NST activation. The result was a significant late-stage decline in both energy expenditure and an inability to protect their body temperature when under chronic cold challenge conditions in the N1—KO mice compared to controls. Nipsnap1 did not appear to affect classical thermogenic effector proteins, but rather interfaced with lipid metabolism which is essential for functional NST [55,56]. *De novo* lipogenesis, as measured by ^{13}C carbon incorporation from ^{13}C labeled glucose into free fatty acids such as palmitic acid was significantly impaired in N1—KO brown adipocytes compared to N1-Flox controls. DNL is critical to provide endogenously generated free fatty acid substrates to fuel beta-oxidation and given that DNL can initiate in the mitochondria though the citrate-malate shuttle, it is possible that Nipsnap1 directly interfaces with this process [57—59]. Impaired DNL likely contributes to the overall defects in the long-term maintenance of NST capacity in the N1—KO mice. Fatty acid beta-oxidation was also significantly impaired in N1—KO primary brown fat cultures as well as in *ex vivo* isolated mitochondria from chronically cold-exposed mice. While this could be a consequence of impaired DNL, the decrease in beta-oxidation enzymes such as Enoyl-CoA hydratase (Echs1) and hydroxyacyl-Coenzyme A (Hadh) would suggest that impairments in beta-oxidation are occurring in parallel with the defects in DNL. This is further supported with our mitochondrial respirometry studies where equal levels of palmitoyl carnitine was provided to isolated mitochondria from the N1—KO mice compared to N1-Flox controls and the defect with beta-oxidation was observed (Figures. S3H and S3I). Curiously, upstream lipid metabolism and regulation was unaltered as both lipid storage and signaling capacities were preserved between the KO and the controls.

The manner in which Nipsnap1 regulates late-stage NST and how it integrates with lipid metabolism however is currently unknown and warrants further investigation. Nipsnap1 is evolutionarily conserved which argues a critical role for the protein, although its specific function, as well as its protein structural domains, have not been completely classified [27]. Reports have indicated that Nipsnap1 can be localized to either the mitochondrial surface [37] or the mitochondrial matrix [29], or both in response to mitochondrial damage [32]. Previous studies have shown that Nipsnap1 can interact with protein co-factors such as p62 and ALFY which are involved in mitophagy and amyloid precursor protein (APP) which is known to regulate mitochondria function [30,36,60]. In this present study, we demonstrate that Nipsnap1 is localized to the mitochondrial matrix in BAT. It is therefore mechanistically plausible that Nipsnap1 could both directly bind and/or directly regulate the function of proteins involved in both DNL and lipid beta-oxidation.

The emerging role of Nipsnap1 however appears to be different when NST is stimulated by the β3 agonist CL 316, 243 in thermoneutrality. Unlike the defects in energy expenditure observed in cold-exposed conditions, Nipsnap1 ablation in the brown fat of N1—KO mice did not alter VO_2 or VCO_2 levels. Instead, the ablation of Nipsnap1 triggered a hyperphagic response in the N1—KO mice compared to N1-Flox controls resulting in an increase in food consumption only in the thermogenic maintenance period when Nipsnap1 is maximally expressed. We hypothesize that this is a compensatory mechanism to couple the increased food intake with increased energy expenditure in order to normalize VO_2 and VCO_2 levels. This mechanism of compensatory has been noted in many other studies and is extremely plausible given that there was no increase in body weight or locomotive movement in the N1—KO mice compared to N1-Flox controls [55,61]. It is also plausible that the defect in energy expenditure and lipid metabolism in N1—KO mice observed under cold-exposed conditions may not be regulated solely through the β3 adrenergic signaling pathway. Indeed cold-induced thermogenesis includes both shivering and non-shivering thermogenesis as well as the activation of multiple pathways apart from just the β3 adrenergic signaling cascade [62,63]. Further experiments are warranted to tease apart the detailed mechanistic interface of the Nipsnap1-lipid metabolism axis under cold-exposed conditions as cold-exposure remains the standard procedure to safely activate NST in humans [64—66].

Ablation of Nipsnap1 did not render the HFD mice more susceptible to diet-induced obesity under TN or cold-exposed environmental conditions. One possibility is that the high fat diet feeding regimen provided more lipid nutrient density and substrates to overcome the lipid metabolism defects in the N1—KO mice that was seen in chow fed conditions compared to N1-Flox controls. Indeed, a study by Nutabi Camargo et al. showed similar findings when high fat diet administration rich in cholesterol and monounsaturated fatty acids was sufficient to overcome lipid metabolism defects [67]. In summary, the findings of this study reveal Nipsnap1 as a critical regulator for the long-term maintenance of non-shivering thermogenesis in BAT. Further studies will be needed in order to discern if targeting Nipsnap1 through overexpression harbors protective benefits in combating obesity and associated metabolic disease.

5. CONCLUSION

In the current study, we identify 4-Nitrophenylphosphatase Domain and Non-Neuronal SNAP25-Like 1 (Nipsnap1) as a critical regulator of long-term thermogenic maintenance in BAT. We demonstrate that the energy expenditure of BAT-specific Nipsnap1 KO mice is significantly reduced during the thermogenic maintenance period and knockout mice are less efficient in maintaining body temperature in a cold environment. Mechanistically, we show that Nipsnap1 regulates lipid metabolism to promote the long-term activation of thermogenesis. Taken together, these studies identify Nipsnap1 as a critical regulator of BAT thermogenic maintenance.

AUTHOR CONTRIBUTIONS

The project was conceptualization, J.J.B. and Y.L.; Methodology, J.J.B., Y.L., and Y.Q.; Investigation, Y.L., Y.Q., C·C., P·C., K.E., and S.X.; Validation, Y.L., S·P., S.E., and N.S. Formal Analysis, J.J.B. and Y.L.; Writing — Original Draft, J.J.B., Y.L., and Y.Q.; Writing — Review & Editing, J.J.B., Y.L., Y.Q., C·C., P·C., K.E., and S.X.; Visualization, J.J.B. and Y.L.; Supervision, J.J.B.

DECLARATION OF COMPETING INTEREST

The authors declare that they have no known competing financial interests or personal relationships that could have appeared to influence the work reported in this paper.

DATA AVAILABILITY

Data will be made available on request.

ACKNOWLEDGMENTS

We acknowledge the Cornell Biotechnology Resource center for the mitoproteomics and whole tissue proteomic analysis. We also sincerely thank E.D.R, L.K, P.C, P.S, K.S, and B.C. for their critical review of the manuscript. A special thanks to R.B. for the figure graphics. This work was funded by NIH NIDDK 5R21DK122258 awarded to J.J.B.

APPENDIX A. SUPPLEMENTARY DATA

Supplementary data to this article can be found online at https://doi.org/10.1016/j.molmet.2023.101770.

REFERENCES

[1] Piché ME, Tchernof A, Després JP. Obesity phenotypes, diabetes, and cardiovascular diseases. Circ Res 2020;126:1477—500. https://doi.org/10.1161/CIRCRESAHA.120.316101.

[2] Panuganti KK, Nguyen M, Kshirsagar RK. Obesity. Antenatal Disorders for the MRCOG and Beyond 2021;135—8.

[3] Pi-Sunyer X. The medical risks of obesity. PGM (Postgrad Med) 2009;121(6):21. https://doi.org/10.3810/PGM.2009.11.2074.

[4] Chobot A, Górowska-Kowolik K, Sokołowska M, Jarosz-Chobot P. Obesity and diabetes—not only a simple link between two epidemics. Diabetes Metabol Res Rev 2018;34(7). https://doi.org/10.1002/DMRR.3042.

[5] Avgerinos KI, Spyrou N, Mantzoros CS, Dalamaga M. Obesity and cancer risk: emerging biological mechanisms and perspectives. Metabolism 2019;92:121—35. https://doi.org/10.1016/J.METABOL.2018.11.001.

[6] Cercato C, Fonseca FA. Cardiovascular risk and obesity. Diabetol Metab Syndrome 2019;11:74. https://doi.org/10.1186/s13098-019-0468-0.

[7] Censin JC, Peters SAE, Bovijn J, Ferreira T, Pulit SL, Mägi R, et al. Causal relationships between obesity and the leading causes of death in women and men. PLoS Genet 2019;15(10):e1008405. https://doi.org/10.1371/JOURNAL.PGEN.1008405.

[8] Bal BS, Finelli FC, Shope TR, Koch TR. Nutritional deficiencies after bariatric surgery. Nat Rev Endocrinol 2012;8(9):544—56. https://doi.org/10.1038/NRENDO.2012.48.

[9] Chang SH, Stoll CRT, Song J, Varela JE, Eagon CJ, Colditz GA. The effectiveness and risks of bariatric surgery: an updated systematic review and meta-analysis, 2003-2012. JAMA Surgery 2014;149(3):275—87. https://doi.org/10.1001/JAMASURG.2013.3654.

[10] Thom G, Lean M. Is there an optimal diet for weight management and metabolic health? Gastroenterology 2017;152(7):1739—51. https://doi.org/10.1053/J.GASTRO.2017.01.056.

[11] Siebenhofer A, Winterholer S, Jeitler K, Horvath K, Berghold A, Krenn C, et al. Long-term effects of weight-reducing drugs in people with hypertension. Cochrane Database Syst Rev 2021;1(1). https://doi.org/10.1002/14651858.CD007654.PUB5.

[12] Rothwell NJ, Stock MJ. A role for Brown adipose tissue in diet-induced thermogenesis. Obes Res 1997;5(6):650—6. https://doi.org/10.1002/J.1550-8528.1997.TB00591.X.

[13] Bartelt A, Bruns OT, Reimer R, Hohenberg H, Ittrich H, Peldschus K, et al. Brown adipose tissue activity controls triglyceride clearance. Nat Med 2011;17(2):200—5. https://doi.org/10.1038/nm.2297. 2011 17:2.

[14] Bordicchia M, Liu D, Amri EZ, Ailhaud G, Dessì-Fulgheri P, Zhang C, et al. Cardiac natriuretic peptides act via p38 MAPK to induce the brown fat thermogenic program in mouse and human adipocytes. J Clin Investig 2012;122(3):1022. https://doi.org/10.1172/JCI59701.

[15] Chen KY, Brychta RJ, Linderman JD, Smith S, Courville A, Dieckmann W, et al. Brown fat activation mediates cold-induced thermogenesis in adult humans in response to a mild decrease in ambient temperature. J Clin Endocrinol Metabol 2013;98(7):E1218. https://doi.org/10.1210/JC.2012-4213.

[16] Lichtenbelt WDVM, Schrauwen P, van de Kerckhove S, Westerterp-Plantenga MS. Individual variation in body temperature and energy expenditure in response to mild cold. Am J Physiol Endocrinol Metab 2002;282(5 45—5):1077—83. https://doi.org/10.1152/AJPENDO.00020.2001. /ASSET/IMAGES/LARGE/H10520818006.JPEG.

[17] Claessens-Van Ooijen AMJ, Westerterp KR, Wouters L, Schoffelen PFM, van Steenhoven AA, van Marken Lichtenbelt WD. Heat production and body temperature during cooling and rewarming in overweight and lean men. Obesity 2006;14(11):1914—20. https://doi.org/10.1038/OBY.2006.223.

[18] Cypess AM, Lehman S, Williams G, Tal I, Rodman D, Goldfine AB, et al. Identification and importance of Brown adipose tissue in adult humans. N Engl J Med 2009;360(15):1509—17. https://doi.org/10.1056/nejmoa0810780.

[19] van Marken Lichtenbelt WD, Vanhommerig JW, Smulders NM, Drossaerts JMAFL, Kemerink GJ, Bouvy ND, et al. Cold-activated Brown adipose tissue in healthy men. N Engl J Med 2009;360(15):1500—8. https://doi.org/10.1056/NEJMOA0808718.

[20] Zingaretti MC, Crosta F, Vitali A, Guerrieri M, Frontini A, Cannon B, et al. The presence of UCP1 demonstrates that metabolically active adipose tissue in the neck of adult humans truly represents brown adipose tissue. Faseb J 2009;23(9):3113—20. https://doi.org/10.1096/FJ.09-133546.

[21] Celi FS, Brychta RJ, Linderman JD, Butler PW, Alberobello AT, Smith S, et al. Minimal changes in environmental temperature result in a significant increase in energy expenditure and changes in the hormonal homeostasis in healthy adults. European Journal of Endocrinology/European Federation of Endocrine Societies 2010;163(6):863. https://doi.org/10.1530/EJE-10-0627.

[22] Hondares E, Rosell M, Gonzalez FJ, Giralt M, Iglesias R, Villarroya F. Hepatic FGF21 expression is induced at birth via PPARα in response to milk intake and

contributes to thermogenic activation of neonatal Brown fat. Cell Metabol 2010;11(3):206–12. https://doi.org/10.1016/J.CMET.2010.02.001.

[23] Seale P, Conroe HM, Estall J, Kajimura S, Frontini A, Ishibashi J, et al. Prdm16 determines the thermogenic program of subcutaneous white adipose tissue in mice. J Clin Invest 2011;121(1):96–105. https://doi.org/10.1172/JCI44271.

[24] Kleiner S, Mepani RJ, Laznik D, Ye L, Jurczak MJ, Jornayvaz FR, et al. Development of insulin resistance in mice lacking PGC-1α in adipose tissues. Proc Natl Acad Sci U S A 2012;109(24):9635–40. https://doi.org/10.1073/PNAS.1207287109.

[25] Roh HC, Tsai LTY, Shao M, Tenen D, Shen Y, Kumari M, et al. Warming induces significant reprogramming of beige, but not Brown, adipocyte cellular identity. Cell Metabol 2018;27(5):1121. https://doi.org/10.1016/J.CMET.2018.03.005.

[26] Leitner BP, Weiner LS, Desir M, Kahn PA, Selen DJ, Tsang C, et al. Kinetics of human brown adipose tissue activation and deactivation. Int J Obes 2019;43(3):633–7. https://doi.org/10.1038/s41366-018-0104-3.

[27] Seroussi E, Pan HQ, Kedra D, Roe BA, Dumanski JP. Characterization of the human NIPSNAP1 gene from 22q12: a member of a novel gene family. Gene 1998;212(1):13–20. https://doi.org/10.1016/S0378-1119(98)00098-5.

[28] Satoh K, Takeuchi M, Oda Y, Deguchi-Tawarada M, Sakamoto Y, Matsubara K, et al. Identification of activity-regulated proteins in the postsynaptic density fraction. Gene Cell 2002;7(2):187–97. https://doi.org/10.1046/J.1356-9597.2001.00505.X.

[29] Nautiyal M, Sweatt AJ, MacKenzie JA, Mark Payne R, Szucs S, Matalon R, et al. Neuronal localization of the mitochondrial protein NIPSNAP1 in rat nervous system. Eur J Neurosci 2010;32(4):560–9. https://doi.org/10.1111/J.1460-9568.2010.07326.X.

[30] Tummala H, Li X, Homayouni R. Interaction of a novel mitochondrial protein, 4-nitrophenylphosphatase domain and non-neuronal SNAP25-like protein homolog 1 (NIPSNAP1), with the amyloid precursor protein family. Eur J Neurosci 2010;31(11):1926–34. https://doi.org/10.1111/j.1460-9568.2010.07248.x.

[31] Morgenstern M, Peikert CD, Lübbert P, Suppanz I, Klemm C, Alka O, et al. Quantitative high-confidence human mitochondrial proteome and its dynamics in cellular context. Cell Metabol 2021;33(12):2464–83. https://doi.org/10.1016/J.CMET.2021.11.001. e18.

[32] Princely Abudu Y, Pankiv S, Mathai BJ, Håkon Lystad A, Bindesbøll C, Brenne HB, et al. NIPSNAP1 and NIPSNAP2 act as "eat me" signals for mitophagy. Dev Cell 2019;49(4):509–25. https://doi.org/10.1016/J.DEVCEL.2019.03.013. e12.

[33] Fathi E, Yarbro JM, Homayouni R. NIPSNAP protein family emerges as a sensor of mitochondrial health. Bioessays 2021:2100014. https://doi.org/10.1002/bies.202100014.

[34] Manisha Nautiyal B, Carolina N, Hutson SM, Poole LB, Mark Payne R, Penn R, et al. A protein in search of function: NIPSNAP1 in mitochondrial branched-chain amino acid metabolon. Brain and apoptosis 2008.

[35] Ghoshal S, Jones L, Homayouni R. NIPSNAP1 deficient mice exhibit altered liver amino acid, lipid and nucleotide metabolism. Metabolomics 2014;10(2):250–8. https://doi.org/10.1007/S11306-013-0583-0/FIGURES/5.

[36] Okuda-Ashitaka E, Minami T, Tsubouchi S, Kiyonari H, Iwamatsu A, Noda T, et al. Identification of NIPSNAP1 as a nocistatin-interacting protein involving pain transmission. J Biol Chem 2012;287(13):10403–13. https://doi.org/10.1074/jbc.M111.271866.

[37] Yamamoto S, Ogasawara N, Yamamoto K, Uemura C, Takaya Y, Shiraishi T, et al. Mitochondrial proteins NIP-SNAP-1 and -2 are a target for the immunomodulatory activity of clarithromycin, which involves NF-κB-mediated cytokine production. Biochem Biophys Res Commun 2017;483(3):911–6. https://doi.org/10.1016/j.bbrc.2016.12.100.

[38] Skarnes WC, Rosen B, West AP, Koutsourakis M, Bushell W, Iyer V, et al. A conditional knockout resource for the genome-wide study of mouse gene function. Nature 2011;474(7351):337–44. https://doi.org/10.1038/nature10163.

[39] Mina AI, LeClair RA, LeClair KB, Cohen DE, Lantier L, Banks AS. CalR: a web-based analysis tool for indirect calorimetry experiments. Cell Metabol 2018;28(4):656–66. https://doi.org/10.1016/J.CMET.2018.06.019. e1.

[40] Wang GX, Meyer JG, Cai W, Softic S, Li ME, Verdin E, et al. Regulation of UCP1 and mitochondrial metabolism in Brown adipose tissue by reversible succinylation. Mol Cell 2019;74(4):844–57. https://doi.org/10.1016/J.MOLCEL.2019.03.021. e7.

[41] Chen EY, Tan CM, Kou Y, Duan Q, Wang Z, Meirelles Gv, et al. Enrichr: interactive and collaborative HTML5 gene list enrichment analysis tool. BMC Bioinf 2013;14:128. https://doi.org/10.1186/1471-2105-14-128.

[42] Kuleshov Mv, Jones MR, Rouillard AD, Fernandez NF, Duan Q, Wang Z, et al. Enrichr: a comprehensive gene set enrichment analysis web server 2016 update. Nucleic Acids Res 2016;44(Web Server issue). https://doi.org/10.1093/NAR/GKW377.

[43] Kraus NA, Ehebauer F, Zapp B, Rudolphi B, Kraus BJ, Kraus D. Quantitative assessment of adipocyte differentiation in cell culture. Adipocyte 2016;5(4):351. https://doi.org/10.1080/21623945.2016.1240137.

[44] Müller S, Balaz M, Stefanicka P, Varga L, Amri EZ, Ukropec J, et al. Proteomic analysis of human Brown adipose tissue reveals utilization of coupled and uncoupled energy expenditure pathways. Sci Rep 2016;6(1):1–9. https://doi.org/10.1038/srep30030. 2016 6:1.

[45] Cantó C, Gerhart-Hines Z, Feige JN, Lagouge M, Noriega L, Milne JC, et al. AMPK regulates energy expenditure by modulating NAD + metabolism and SIRT1 activity. Nature 2009;458(7241):1056–60. https://doi.org/10.1038/nature07813.

[46] Ferrick DA, Neilson A, Beeson C. Advances in measuring cellular bioenergetics using extracellular flux. Drug Discov Today 2008:268–74. https://doi.org/10.1016/j.drudis.2007.12.008.

[47] Rothwell NJ, Stock MJ. A role for brown adipose tissue in diet-induced thermogenesis. Nature 1979;281.

[48] Warwick PM, Busby R. Influence of mild cold on 24 h energy expenditure in "normally" clothed adults. Br J Nutr 1990;63(3):481–8. https://doi.org/10.1079/BJN19900135.

[49] Kazak L, Chouchani ET, Jedrychowski MP, Erickson BK, Shinoda K, Cohen P, et al. A creatine-driven substrate cycle enhances energy expenditure and thermogenesis in beige fat. Cell 2015;163(3):643–55. https://doi.org/10.1016/j.cell.2015.09.035.

[50] Mills EL, Pierce KA, Jedrychowski MP, Garrity R, Winther S, Vidoni S, et al. Accumulation of succinate controls activation of adipose tissue thermogenesis. Nature 2018;560(7716):102–6. https://doi.org/10.1038/s41586-018-0353-2.

[51] Rahbani JF, Roesler A, Hussain MF, Samborska B, Dykstra CB, Tsai L, et al. Creatine kinase B controls futile creatine cycling in thermogenic fat. Nature 2021;590. https://doi.org/10.1038/s41586-021-03221-y.

[52] Sun Y, Rahbani JF, Jedrychowski MP, Riley CL, Vidoni S, Bogoslavski D, et al. Mitochondrial TNAP controls thermogenesis by hydrolysis of phosphocreatine. Nature 2021;580:593. https://doi.org/10.1038/s41586-021-03533-z.

[53] Lean MEJ, Murgatroyd PR, Rothnie I, Reid IW, Harvey R. Metabolic and thyroidal responses to mild cold are abnormal in obese diabetic women. Clin Endocrinol 1988;28(6):665–73. https://doi.org/10.1111/J.1365-2265.1988.TB03859.X.

[54] Deng J, Neff LM, Rubert NC, Zhang B, Shore RM, Samet JD, et al. MRI characterization of brown adipose tissue under thermal challenges in normal weight, overweight, and obese young men. J Magn Reson Imag 2018;47(4):936–47. https://doi.org/10.1002/JMRI.25836.

[55] Adlanmerini M, Carpenter BJ, Remsberg JR, Aubert Y, Peed LC, Richter HJ, et al. Circadian lipid synthesis in brown fat maintains murine body temperature during chronic cold. Proc Natl Acad Sci U S A 2019;116(37):18691–9. https://doi.org/10.1073/PNAS.1909883116/-/DCSUPPLEMENTAL.

[56] Calderon-Dominguez M, Mir JF, Fucho R, Weber M, Serra D, Herrero L. Fatty acid metabolism and the basis of brown adipose tissue function. Adipocyte 2016;5(2):98. https://doi.org/10.1080/21623945.2015.1122857.

[57] Mottillo EP, Balasubramanian P, Lee Y-H, Weng C, Kershaw EE, Granneman JG. Coupling of lipolysis and de novo lipogenesis in brown, beige, and white adipose tissues during chronic β3-adrenergic receptor activation. JLR (J Lipid Res) 2014;55(11):2276–86. https://doi.org/10.1194/jlr.M050005.

[58] Trayhurn P. Fatty acid synthesis in mouse brown adipose tissue the influence of environmental temperature on the proportion of whole-body fatty acid synthesis in brown adipose tissue and the liver. Biochim Biophys Acta Lipids Lipid Metabol 1981;664(3):549–60. https://doi.org/10.1016/0005-2760(81)90132-6.

[59] Song Z, Xiaoli A, Yang F. Regulation and metabolic significance of de novo lipogenesis in adipose tissues. Nutrients 2018;10(10):1383. https://doi.org/10.3390/nu10101383.

[60] Abudu YP, Pankiv S, Mathai BJ, Lamark T, Johansen T, Simonsen A. NIPSNAP1 and NIPSNAP2 act as "eat me" signals to allow sustained recruitment of autophagy receptors during mitophagy. Autophagy 2019:1845–7. https://doi.org/10.1080/15548627.2019.1637642.

[61] LeBlanc J, Labrie A. A possible role for palatability of the food in diet-induced thermogenesis. Int J Obes 1997;21(12):1100–3. https://doi.org/10.1038/sj.ijo.0800520. 1997 21:12.

[62] Cannon B, Nedergaard J. Nonshivering thermogenesis and its adequate measurement in metabolic studies. J Exp Biol 2011;214(Pt 2):242–53. https://doi.org/10.1242/JEB.050989.

[63] Cohen P, Spiegelman BM. Brown and beige fat: molecular parts of a thermogenic machine. Diabetes 2015;64(7):2346. https://doi.org/10.2337/DB15-0318.

[64] Ahmed BA, Varah N, Ong FJ, Blondin DP, Gunn E, Konyer NB, et al. Impaired cold-stimulated supraclavicular Brown adipose tissue activity in young boys with obesity. Diabetes 2022;71(6):1193–204. https://doi.org/10.2337/DB21-0799.

[65] Orava J, Nuutila P, Lidell ME, Oikonen V, Noponen T, Viljanen T, et al. Different metabolic responses of human brown adipose tissue to activation by cold and insulin. Cell Metabol 2011;14(2):272–9. https://doi.org/10.1016/j.cmet.2011.06.012.

[66] Rosenbaum M, Leibel RL. Adaptive thermogenesis in humans. Int J Obes 2010;34:S47–55. https://doi.org/10.1038/ijo.2010.184.

[67] Camargo N, Brouwers JF, Loos M, Gutmann DH, Smit AB, Verheijen MHG. High-fat diet ameliorates neurological deficits caused by defective astrocyte lipid metabolism. Faseb J 2012;26(10):4302–15. https://doi.org/10.1096/FJ.12-205807.

